

This article may be downloaded for personal use only. Any other use requires prior permission of the author and AIP Publishing.

The following article appeared in *Applied Physics Letters* 103, 152401 (2013); and may be found at <https://doi.org/10.1063/1.4824073>

Texture-induced enhancement of the magnetocaloric response in melt-spun DyNi₂ ribbons

P. J. Ibarra-Gaytan, C. F. Sánchez-Valdes, J. L. Sánchez Llamazares, Pablo Álvarez-Alonso, Pedro Gorria, and J. A. Blanco

Citation: *Appl. Phys. Lett.* **103**, 152401 (2013);

View online: <https://doi.org/10.1063/1.4824073>

View Table of Contents: <http://aip.scitation.org/toc/apl/103/15>

Published by the [American Institute of Physics](#)

Articles you may be interested in

[Enhanced refrigerant capacity in two-phase nanocrystalline/amorphous NdPrFe₁₇ melt-spun ribbons](#)

Applied Physics Letters **104**, 212401 (2014); 10.1063/1.4879544

[Magnetic entropy change and refrigerant capacity of rapidly solidified TbNi₂ alloy ribbons](#)

Journal of Applied Physics **113**, 17A912 (2013); 10.1063/1.4794988

[Two successive magnetic transitions induced large refrigerant capacity in HoPdIn compound](#)

Applied Physics Letters **103**, 222405 (2013); 10.1063/1.4834815

[Giant reversible magnetocaloric effect in ErMn₂Si₂ compound with a second order magnetic phase transition](#)

Applied Physics Letters **100**, 152403 (2012); 10.1063/1.4704155

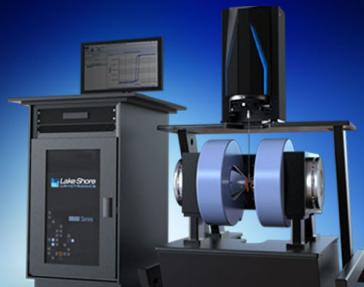
[Large reversible magnetocaloric effect in a Ni-Co-Mn-In magnetic shape memory alloy](#)

Applied Physics Letters **108**, 032405 (2016); 10.1063/1.4940441

[Magnetic entropy table-like shape in RNi₂ composites for cryogenic refrigeration](#)


Journal of Applied Physics **117**, 17C116 (2015); 10.1063/1.4915480

 **Lake Shore**
CRYOTRONICS



8600 Series VSM

For fast, highly sensitive
measurement performance

LEARN MORE 

Texture-induced enhancement of the magnetocaloric response in melt-spun DyNi₂ ribbons

P. J. Ibarra-Gaytan,¹ C. F. Sánchez-Valdes,¹ J. L. Sánchez Llamazares,^{1,a)}
 Pablo Álvarez-Alonso,² Pedro Gorria,³ and J. A. Blanco⁴

¹Instituto Potosino de Investigación Científica y Tecnológica, Camino a la Presa San José 2055,
 Col. Lomas 4^a, San Luis Potosí S.L.P. 78216, Mexico

²Departamento de Electricidad y Electrónica, Universidad del País Vasco (UPV/EHU), 48940 Leioa, Spain

³Departamento de Física, EPI, Universidad de Oviedo, 33230 Gijón, Spain

⁴Departamento de Física, Universidad de Oviedo, Calvo Sotelo s/n, 33007 Oviedo, Spain

(Received 22 June 2013; accepted 18 September 2013; published online 7 October 2013)

The magnetocaloric properties of melt-spun ribbons of the Laves phase DyNi₂ have been investigated. The as-quenched ribbons crystallize in a single-phase MgCu₂-type crystal structure (C15; space group $Fd\bar{3}m$) exhibiting a saturation magnetization and Curie temperature of $M_S = 157 \pm 2 \text{ A m}^2 \text{ kg}^{-1}$ and $T_C = 21.5 \pm 1 \text{ K}$, respectively. For a magnetic field change of 2 T, ribbons show a maximum value of the isothermal magnetic entropy change $|\Delta S_M^{\text{peak}}| = 13.5 \text{ J kg}^{-1} \text{ K}^{-1}$, and a refrigerant capacity $RC = 209 \text{ J kg}^{-1}$. Both values are superior to those found for bulk polycrystalline DyNi₂ alloys (25% and 49%, respectively). In particular, the RC is comparable or larger than that reported for other potential magnetic refrigerants operating at low temperatures, making DyNi₂ ribbons promising materials for use in low-temperature magnetic refrigeration applications. © 2013 AIP Publishing LLC. [<http://dx.doi.org/10.1063/1.4824073>]

Over the last two decades, the magnetocaloric (MC) properties of Laves phases have been extensively investigated. As a result, some compounds in the RCo₂, RAl₂, and RNi₂ systems (R = rare earth) have been referred to as promising magnetic refrigerants in the 10–80 K temperature range.^{1,2} In particular, RNi₂ with R = Tb, Dy, or Er and related compounds have been proposed as suitable components to design a low-temperature magnetocaloric composite with a “table-like” temperature dependence of the isothermal magnetic entropy change $\Delta S_M(T)$.^{2–4} Such a table-like shape of $\Delta S_M(T)$ is an essential requisite for an ideal Ericsson-like refrigeration cycle.⁵ Therefore, the development of MC multiphase materials or composites with improved refrigerant capacity, RC , compared to the individual components is currently a hot topic in the field of magnetic refrigeration in different temperature ranges.^{6–9} Early theoretical calculations of the MC properties performed on the DyNi₂ compound, which were based on a Hamiltonian that considered the exchange magnetic interactions in the molecular field approximation and the crystalline electrical-field anisotropy, predicted a large maximum magnetic entropy change ΔS_M^{peak} of $\sim -5.9 \text{ J mol}^{-1} \text{ K}^{-1}$ ($-21.1 \text{ J kg}^{-1} \text{ K}^{-1}$) and $\sim -4.0 \text{ J mol}^{-1} \text{ K}^{-1}$ ($-14.3 \text{ J kg}^{-1} \text{ K}^{-1}$) under magnetic field changes $\mu_0 \Delta H$ of 5 T and 2 T, respectively. These values were close to those found for bulk alloys (-5.9 and $-3.8 \text{ J mol}^{-1} \text{ K}^{-1}$, respectively).¹⁰ Recently, a theoretical model including both crystal-field and exchange interactions that considers the effect of magnetic fluctuations has been reported, which satisfactorily accounts for the experimental $\Delta S_M(T)$ curve of DyNi₂.¹¹

The intermetallic compound DyNi₂ is a cubic Laves phase that crystallizes either in a MgCu₂-type crystal structure (C15,

space group $Fd\bar{3}m$),^{12–15} or in a superstructure of C15 (space group $F\bar{4}3m$) with a doubled a -axis compared to the former.^{16–18} In this compound, only the Dy⁺³ ions possess a magnetic moment,¹² being a ferromagnet with a Curie temperature, $T_C = 21.5 \text{ K}$,^{10,18,19} and the easy magnetization axis along the [100] direction.²⁰

Until now, the DyNi₂ compound has been prepared using conventional melting techniques (arc or RF melting) followed by long-term annealing (from several days to a month) at temperatures between 723 and 1073 K.^{12,15,18} Rapid solidification using the melt spinning technique has been effectively applied to produce different crystalline magnetocaloric materials, such as LaFe_{13–x}Si_x,²¹ MnCoGe (Ref. 22) (MnFe)₂(PGe),²³ Gd₅(SiGeSn)₄,²⁴ TbNi₂,²⁵ and Ni-Mn-X Heusler alloys (X = Sn, In, Ga),^{26–28} In all of the above-mentioned cases, a single phase was found in the as-quenched alloy ribbons, or after a much shortened annealing compared to their bulk counterparts. Hence, the aim of the present investigation has been to study the phase constitution and MC behavior of DyNi₂ as-quenched (aq) ribbons; the results are compared with those obtained for bulk samples produced by conventional alloying techniques.

Bulk alloys of nominal composition DyNi₂ were produced by arc melting from pure elements (Dy 99.9% and Ni 99.99% purity) under a controlled Ar atmosphere. Samples were melted several times to ensure an adequate starting homogeneity. Polycrystalline alloy ribbons (thickness of ≈ 18 – $22 \mu\text{m}$) were fabricated using a homemade melt spinning system operating in an Ar environment at a copper wheel speed of 25 ms^{-1} .

X-ray diffraction (XRD) patterns of finely powdered samples were collected with a Bruker AXS model D8 Advance X-ray powder diffractometer using Cu-K α radiation ($\lambda = 1.5418 \text{ \AA}$). The scan was carried out in the interval $25^\circ \leq 2\theta \leq 95^\circ$ with 0.02° steps increments at a counting rate

^{a)}Author to whom correspondence should be addressed. Electronic mail: jose.sanchez@ipicyt.edu.mx

of 20 s per step. Microstructure and elemental composition were determined with a FEI/Philips XL30 FEG ESEM equipped with an energy dispersive spectroscopy (EDS) system. Magnetic measurements were performed by vibrating sample magnetometry in a Quantum Design PPMS® EverCool®-9T platform, in which the magnetic field $\mu_0 H$ was applied along the ribbon axis (i.e., the rolling direction) to minimize the effect of the demagnetizing field. The low-field (5 mT) magnetization curve as a function of temperature $M(T)$ was measured between 2 and 40 K in order to estimate the value of T_C . In addition, the high-field $M(T)$ curve was measured under $\mu_0 H = 5$ T. A set of isothermal magnetization curves, $M(\mu_0 H)$, was collected every 1.5 K from 6.5 K to 54 K up to a maximum applied magnetic field of 5 T. At each temperature, the magnetization under a large number of selected magnetic field values was measured to improve the accuracy in the calculation of the isothermal magnetic entropy change, ΔS_M . The value of ΔS_M at each temperature T , due to a change of the applied magnetic field from $\mu_0 H = 0$ to $\mu_0 H_{\max}$, was calculated using the Maxwell relation

$$\Delta S_M(T, \mu_0 H) = \mu_0 \int_0^{\mu_0 H_{\max}} \left(\frac{\partial M(\mu_0 H, T)}{\partial T} \right)_{H'} dH'.$$

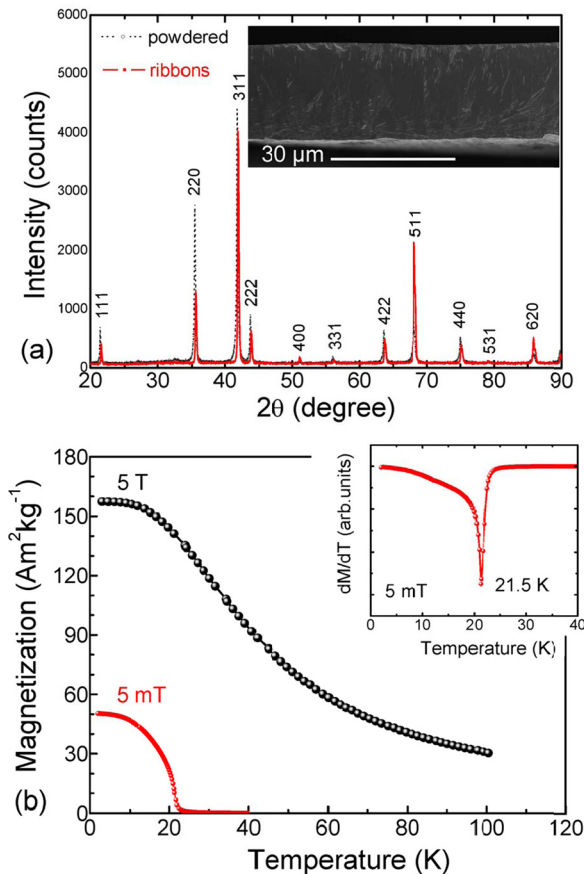


FIG. 1. (a) Room temperature x-ray powder diffraction pattern of DyNi_2 , in powdered and ribbon forms. Inset: typical cross-sectional microstructure of DyNi_2 ribbons. (b) $M(T)$ curves measured in the field-cooled regime at 5 mT (full red symbols), and 5 T (open symbols). Inset: the dM/dT versus T curve at 5 mT, where the Curie temperature $T_C = 21.5 \pm 1$ K is indicated.

In order to estimate the RC values from the $\Delta S_M(T)$ curves, three different methods are conventionally used: (a) by finding the product $|\Delta S_M^{\text{peak}}| \times \delta T_{\text{FWHM}}$ (hereafter referred to as $RC-1$),⁵ where $\delta T_{\text{FWHM}} = T_{\text{hot}} - T_{\text{cold}}$ is the temperature range that corresponds to the full width at half maximum of the $\Delta S_M(T)$ curve (here, δT_{FWHM} coincides with the temperature span of the thermodynamic cycle); (b) by calculating the integral, under the $\Delta S_M(T)$ curves between T_{hot} and T_{cold} (hereafter referred to as $RC-2$),²⁹ and (c) by maximizing the product $\Delta S_M \times \delta T$ below the $\Delta S_M(T)$ curve (referred to as $RC-3$).³⁰

The magnetocaloric effect of bulk polycrystalline DyNi_2 has been calculated from heat capacity measured as a function of temperature under applied magnetic field values of 0, 2, and 5 T using a semi-adiabatic heat pulse calorimeter³¹ as described in Ref. 32. The sample for these measurements has been prepared by arc-melting of stoichiometric amounts of Dy (better than 99.8 at. % pure with respect to all elements in the periodic table (Materials Preparation Center of Ames Laboratory, <https://www.ameslab.gov/mpc>) and Ni (99.99% pure).

The room temperature XRD pattern of the as-quenched ribbons is depicted in Figure 1(a). All of the observed diffraction peaks can be satisfactorily indexed as the Bragg reflections corresponding to the MgCu_2 -type crystal structure of the Laves phase ($C15$, space group $Fd\bar{3}m$), with a refined

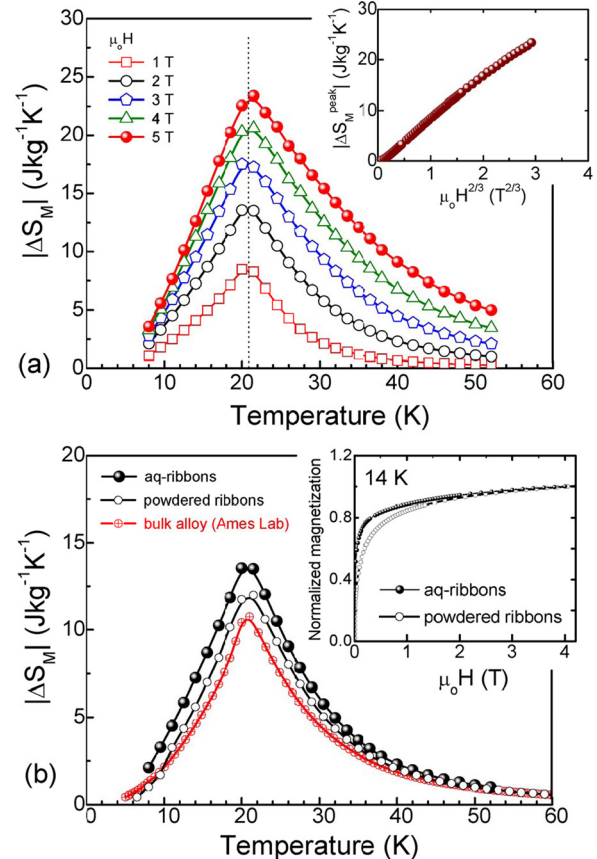


FIG. 2. (a) Temperature dependence of the magnetic entropy change $\Delta S_M(T)$ under $\mu_0 H = 1, 2, 3, 4,$ and 5 T. Inset: $|\Delta S_M^{\text{peak}}|$ as a function of $(\mu_0 H)^{2/3}$. (b) Comparison of the $|\Delta S_M(T)|$ curves for the as-quenched (aq) and powdered ribbons together with that corresponding to the polycrystalline bulk alloy. Inset: Magnetic field dependence of the normalized magnetization for the as-quenched and powdered ribbons.

TABLE I. Maximum value of the magnetic entropy change $|\Delta S_M^{\text{peak}}|$, refrigerant capacities $RC-1$, $RC-2$, and $RC-3$, and related temperature parameters for magnetic field changes of 2 T and 5 T for as-quenched ribbons, and bulk polycrystalline samples, of the intermetallic compound DyNi_2 . For the sake of comparison, the magnetocaloric properties of the intermetallic compound Er_3Ni_3 are also listed (see Ref. 35); this material shows the same working temperature range than the one shown by the aq DyNi_2 alloy ribbons.

	As-quenched ribbons		Bulk polycrystalline alloys		Er_3Ni_3 (Ref. 35) ^a	
	$\mu_0\Delta H$ (T)		$\mu_0\Delta H$ (T)		$\mu_0\Delta H$ (T)	
	2 T	5 T	2 T	5 T	2 T	5 T
$ \Delta S_M^{\text{peak}} $ ($\text{J kg}^{-1} \text{K}^{-1}$)	13.5	23.5	10.7	21.1	10.8 ^a	19.5 ^a
$RC-1$	209	519	140	443	173 ^a	487 ^a
$RC-2$	160	390	102	332	144 ^a	392 ^a
δT_{FWHM} (K)	16	23	13	20	16 ^a	25 ^a
T_{hot} (K)	29	36	28	35	25	35
T_{cold} (K)	13	13	15	14	9	10
$RC-3$	105	260
δT^{RC-3} (K)	17	23
T_{hot} (K) ^b	30	36
T_{cold} (K) ^b	13	13

^aEstimated value from the $\Delta S_M(T)$ curve reported.

^bRelated to $RC-3$.

lattice parameter $a = 7.162 \text{ \AA} \pm 0.001 \text{ \AA}$, which is similar to those reported for bulk alloys.^{13–15} The inset of Figure 1(a) shows a typical SEM micrograph of the ribbon's fracture microstructure. The image reveals micron-size columnar grains with a tendency to grow along the entire ribbon thickness, with the longer axis perpendicular to the ribbon plane. EDS analyses performed on the cross section and both ribbon surfaces for different ribbon flakes indicate that the chemical composition is consistent (with an uncertainty of $\sim 0.1\%$ wt.) with that of the starting bulk alloy ($\approx 1:2$, Dy:Ni).

Figure 1(b) shows the temperature dependence of the magnetization, $M(T)$, measured under applied magnetic field values of 5 mT (red closed circles) and 5 T (black open circles). The Curie temperature, $T_C = 21.5 \pm 1 \text{ K}$, was estimated from the low-field $M(T)$ curve as the minimum of the dM/dT versus T variation (see inset), and the saturation magnetization, $M_S = 157 \pm 2 \text{ A m}^2 \text{ kg}^{-1}$ at $T = 2 \text{ K}$, was estimated from an approach-to-saturation law. Both T_C and M_S are in good agreement with the values reported for bulk alloys.^{10,18,19}

Figure 2(a) shows the $\Delta S_M(T)$ curves for DyNi_2 ribbons for magnetic field changes ranging from 1 to 5 T, while the dependence of $|\Delta S_M^{\text{peak}}|$ on $(\mu_0 H)^{2/3}$ is given in the inset. The latter is consistent with the description given in Ref. 33 for MC materials with second-order magnetic phase transitions. In addition, we compare the $\Delta S_M(T)$ curves ($\mu_0\Delta H = 2$ and 5 T) for both the as-quenched ribbon and the bulk alloy (see Table I for a summary of the MC data). For $\mu_0\Delta H = 2 \text{ T}$, the as-quenched ribbons exhibit a high value for the maximum magnetic entropy change $|\Delta S_M^{\text{peak}}| = 13.5 \text{ J kg}^{-1} \text{ K}^{-1}$ at 21.5 K, as well as a full width at half maximum for the $|\Delta S_M(T)|$ curve of $\delta T_{FMHW} = 16 \text{ K}$ (between 13 and 29 K). It is important to note that $|\Delta S_M^{\text{peak}}|$ is 25% higher than the value attained for the bulk polycrystalline sample, for which $|\Delta S_M^{\text{peak}}| = 10.7 \text{ J kg}^{-1} \text{ K}^{-1}$ ($\mu_0\Delta H = 2 \text{ T}$).

A simple explanation results immediately from the microstructure of DyNi_2 ribbon samples and their magnetic

properties. DyNi_2 is known to have an anisotropic magnetic response, where the [100] direction is the easy magnetization direction ($9 \mu_B$ under 4 T), while the [111] direction is the hardest one ($5 \mu_B$ under 4 T).²⁰ This leads to anisotropic MCE behavior, where the difference in the isothermal magnetic entropy between [100] and [111] directions reaches values of 4 J/kg K for $\mu_0\Delta H = 2 \text{ T}$.³⁴ On the other hand, the X-ray pattern [see Fig. 1(a)] provides evidence that the ribbons are clearly textured, thus it seems likely that the special MC properties of DyNi_2 ribbons could be related to a combination of texture effects (extrinsic feature) and anisotropic MCE response (intrinsic feature). In order to get a qualitative verification of such an assertion, we pulverized some pieces of the as-quenched ribbon to measure the MC response as well as the powder diffraction pattern. It can be observed in Fig. 1(a) that the relative intensity of some reflections changes markedly between the as-quenched ribbon and the

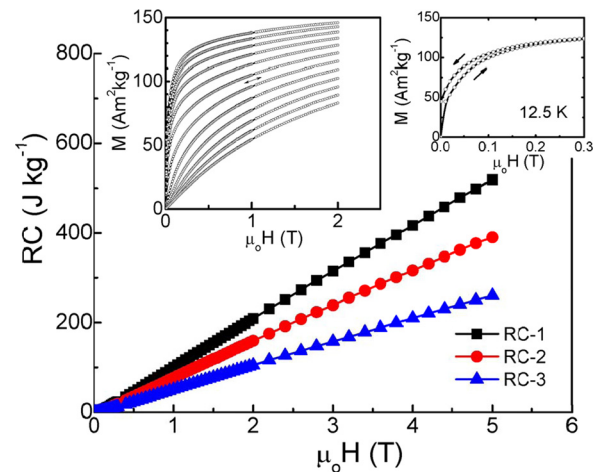


FIG. 3. Field dependence of the refrigerant capacity $RC-1$, $RC-2$, and $RC-3$ (see the text for definition). Left inset: magnetization isotherms under increasing and decreasing the field up to $\mu_0\Delta H = 2 \text{ T}$ in the temperature range between 12.5 and 29 K (i.e., δT_{FWHM}). Right inset: low-field region of the curves measured at 12.5 K.

TABLE II. Transition temperature (T_{trans}), peak value of the magnetic entropy change $|\Delta S_{\text{M}}^{\text{peak}}|$ (absolute value), refrigerant capacity $RC-1$, and δT_{FWHM} , for magnetic field changes of 2 T and 5 T for melt spun and bulk ribbon samples of DyNi₂ and those reported for different materials with large refrigerant capacity in a similar temperature range. Abbreviations: FM = ferromagnetic; PM = paramagnetic; AFM = antiferromagnetic.

Material	T_{trans} (K)	$ \Delta S_{\text{M}}^{\text{peak}} $ (J kg ⁻¹ K ⁻¹)		$RC-1$ (J kg ⁻¹)		δT_{FWHM} (K)		Transition type	References
		2 T	5 T	2 T	5 T	2 T	5 T		
DyNi ₂ ribbons	21.5	13.5	23.5	209	519	15.5	22.1	FM-PM	Present work
DyNi ₂ -bulk	21	10.7 ^a	21.2 ^a	140 ^a	434 ^a	13	20	FM-PM	10 and 11 ^b
TbCoC ₂	28	7.8 ^a	15.3 ^a	109 ^a	367 ^a	14	24	FM-PM	36
GdCo ₂ B ₂	25	9.3 ^a	17.1 ^a	83.7 ^a	478 ^a	9	28	AFM-FM	37
Er ₃ Ni ₂	16	10.8 ^a	19.5 ^a	173 ^a	487 ^a	16	25	FM-PM	35
Er ₃ Co	15	9 ^a	17.1 ^a	135 ^a	442 ^a	15	26	FM-PM	38
HoNi ₂	13	24 ^a	33 ^a	216 ^a	528 ^a	9	16	FM-PM	39
DySb	11	...	15.6 ^a	...	140 ^a	...	9	AFM-FM	40
HoCuSi	9	17 ^a	33 ^a	136 ^a	495 ^a	8	15	AFM-FM	41
ErNi ₂	7	11.2 ^a	20.3 ^a	100 ^a	324 ^a	9	16	...	39
Ho ₃ Ni ₂	33	9.7 ^a	21.7 ^a	165 ^a	477 ^a	17	22	FM-PM	37
NdMn ₂ Ge _{0.4} Si _{1.6}	36	12.3 ^a	18 ^a	111 ^a	270 ^a	9	15	AFM-FM	42

^aEstimated value from the $\Delta S_{\text{M}}(T)$ curve reported.

^bPapers in which theoretical and experimental data are compared.

powdered ribbon. Moreover, if we look at Fig. 2(b), it is clearly perceived that the value of the $|\Delta S_{\text{M}}^{\text{peak}}|$ of the powdered sample is reduced with respect to that of the as-quenched ribbon, being around 10% higher than that measured in the bulk alloy. These findings indicate that at least part of the texture effects induced during the melt-spinning fabrication process have been released upon mechanical pulverization. Furthermore, it seems that the melt-spinning procedure favors the growth of most of the crystalline domains with their (100) planes aligned close to the rolling direction (as the inset of Fig. 2(b) shows the magnetization isotherms show a faster approach to saturation for the aq ribbons), thus enhancing the magnetic entropy change of about 25% with respect to the polycrystalline bulk alloy, where the crystalline domains are assumed to be randomly distributed.

Figure 3 displays the magnetic-field dependence of the refrigerant capacities $RC-1$, $RC-2$, and $RC-3$ for the as-quenched ribbon up to $\mu_0\Delta H_{\text{max}} = 5$ T. It is worth noting that $RC-2$ for $\mu_0\Delta H = 2$ T is increased by 49% with respect to the bulk sample (see Table I), which arises from a combination of enlarged $|\Delta S_{\text{M}}^{\text{peak}}|$ and a broadening of the $|\Delta S_{\text{M}}(T)|$ curve. Therefore, the values for the refrigerant capacity of DyNi₂ as-quenched ribbons are comparable or even larger than those already reported in different materials, with first- and second-order magnetic phase transitions, which have been referred to as promising magnetic refrigerants in the same temperature range. For the sake of comparison, their transition temperature T_{trans} , together with the values of $|\Delta S_{\text{M}}^{\text{peak}}|$, $RC-1$, and δT_{FWHM} under a magnetic field change of 2 T and 5 T are compared with those of DyNi₂ aq-ribbons in Table II. In Table I, we also list the magnetocaloric properties of the intermetallic compound Er₂Ni₃³⁵ since it shows the same working temperature range than the one exhibited by aq DyNi₂ alloy ribbons.

Regarding RC for a specific material, an important consideration is the existence of hysteresis losses due to the irreversible behavior of the field dependence of magnetization within the operating temperature range δT_{FWHM} (particularly

in the ferromagnetic region), since they result in heat release reducing its effective refrigerant capacity (for a certain temperature, the hysteresis loss is given by the area enclosed between the magnetization curve measured under increasing-decreasing magnetic field).

The $M(\mu_0H)$ curves measured for DyNi₂ ribbons from 12.5 to 29 K are shown in the upper left inset of Figure 3. As can be observed, they are almost reversible. In the right inset of Figure 3, the low-field region of the $M(\mu_0H)$ curve measured under increasing-decreasing magnetic field at $T = 12.5$ K (i.e., at T_{cold}) has been plotted. An irreversible behavior is observed for $\mu_0\Delta H < 0.15$ T, which gives rise to a negligible hysteresis loss smaller than ~ 1 J kg⁻¹.

In summary, single-phase alloy ribbons of the Laves phase DyNi₂ with the MgCu₂-type crystal structure have been obtained by means of a one-step melt spinning solidification technique. The samples exhibit a large and almost reversible magnetocaloric effect with a largely enhanced refrigerant capacity well above the one found in bulk polycrystalline alloy, owing to the texture induced in the ribbon during fabrication. Moreover, the magnitudes for the peak value of the magnetic entropy change and the refrigerant capacity of the DyNi₂ ribbons are among the larger values reported for materials with second- and first-order magnetic transitions at low temperatures. These findings make DyNi₂ alloy ribbons promising materials for low-temperature magnetic refrigeration and can boost the use of out-of-equilibrium fabrication procedures for improving the performance of the magnetocaloric materials already known.

Magnetocaloric effect data of bulk DyNi₂ have been kindly provided by Dr. V. K. Pecharsky and Dr. K. A. Gschneidner, Jr. of the United States Department of Energy Ames Laboratory. We truly appreciate the valuable comments made by Dr. V. K. Pecharsky, which really helped us to improve the manuscript. The authors acknowledge the financial support received from: (a) CONACYT, Mexico, under Project No. CB-2010-01-156932; (b) the Spanish MINECO for financial support under Project No.

MAT2011-27573-C04, and from the Basque Government (IT-347-07); and Laboratorio Nacional de Investigaciones en Nanociencias y Nanotecnología (LINAN, IPICYT). Technical support from M.Sc. G. J. Labrada-Delgado is recognized. C.F.S.V. thanks CSIC, Spain, for supporting his Ph.D. studies (Grant No. JAEPRE-08-00508).

- ¹K. A. Gschneidner, Jr., K. Pecharsky, and A. O. Tsokol, *Rep. Prog. Phys.* **68**, 1479 (2005).
- ²N. A. de Oliveira and P. J. von Ranke, *Phys. Rep.* **489**, 89 (2010).
- ³P. J. von Ranke, D. F. Grangeia, A. Caldas, and N. A. de Oliveira, *J. Appl. Phys.* **93**, 4055 (2003).
- ⁴L. Li, M. Kadohaga, V. Franco, Z. Qian, and T. Namiki, *Appl. Phys. Lett.* **101**, 122401 (2012).
- ⁵A. M. Tishin and Y. I. Spichkin, *The Magnetocaloric Effect and its Applications* (IOP, Bristol, 2003).
- ⁶R. Caballero-Flores, V. Franco, A. Conde, K. E. Kipling, and M. A. Willard, *Appl. Phys. Lett.* **98**, 102505 (2011).
- ⁷P. Álvarez, J. L. Sánchez Llamazares, P. Gorria, and J. A. Blanco, *Appl. Phys. Lett.* **99**, 232501 (2011).
- ⁸V. Franco, J. S. Blazquez, B. Ingale, and A. Conde, *Annu. Rev. Mater. Res.* **42**, 305 (2012).
- ⁹P. Álvarez, P. Gorria, J. L. Sánchez Llamazares, and J. A. Blanco, *J. Alloys Compd.* **568**, 98 (2013).
- ¹⁰P. J. von Ranke, V. K. Pecharsky, and K. A. Gschneidner, Jr., *Phys. Rev. B* **58**, 12110 (1998).
- ¹¹P. Álvarez, P. Gorria, and J. A. Blanco, *Phys. Rev. B* **84**, 024412 (2011).
- ¹²E. A. Skrabek and W. E. Wallace, *J. Appl. Phys.* **34**, 1356 (1963).
- ¹³O. D. McMasters and K. A. Gschneidner, *Nucl. Metall.* **10**, 93 (1964).
- ¹⁴H. Oesterreicher, J. Stanley, and R. Pitts, *Phys. Status Solidi A* **12**, K65 (1972).
- ¹⁵R. L. Cohen, K. W. West, F. Oliver, and K. H. J. Buschow, *Phys. Rev. B* **21**, 941 (1980).
- ¹⁶M. Lacroche, V. Paul-Boncour, A. Percheron-Guegan, and J. C. Achard, *J. Less-Common Met.* **161**, L27 (1990).
- ¹⁷M. Lacroche, V. Paul-Boncour, and A. Percheron-Guegan, *Z. Phys. Chem.* **179**, 261 (1993).
- ¹⁸J. Cwik, T. Palewski, K. Nenkov, J. Lyubina, J. Warchulska, J. Klamut, and O. Gutfleisch, *J. Magn. Magn. Mater.* **321**, 2821 (2009).
- ¹⁹A. S. Markosyan, *Fiz. Tverd. Tela* **23**, 1153 (1981).
- ²⁰D. Gignoux and F. Givord, *Solid State Commun.* **21**, 499 (1977).
- ²¹O. Gutfleisch, A. Yan, K.-H. Müller, and L. Schultz, *J. Appl. Phys.* **97**, 10M305 (2005).
- ²²C. F. Sánchez-Valdés, J. L. Sánchez Llamazares, H. Flores-Zúñiga, D. Ríos-Jara, P. Álvarez-Alonso, and P. Gorria, *Scr. Mater.* **69**, 211 (2013).
- ²³A. Yan, K.-H. Müller, L. Schultz, and O. Gutfleisch, *J. Appl. Phys.* **99**, 08K903 (2006).
- ²⁴T. Zhang, Y. Chen, and Y. Tang, *J. Phys. D: Appl. Phys.* **40**, 5778 (2007).
- ²⁵J. L. Sánchez Llamazares, C. F. Sánchez-Valdés, P. J. Ibarra-Gaytan, P. Álvarez-Alonso, P. Gorria, and J. A. Blanco, *J. Appl. Phys.* **113**, 17A912 (2013).
- ²⁶B. Hernando, J. L. Sánchez Llamazares, V. Prida, D. Baldomir, D. Serantes, M. Ilyn, and J. González, *Appl. Phys. Lett.* **94**, 222502 (2009).
- ²⁷J. L. Sánchez Llamazares, H. Flores-Zúñiga, C. F. Sánchez-Valdés, C. A. Ross, and C. García, *J. Appl. Phys.* **111**, 07A932 (2012).
- ²⁸Z. B. Li, J. L. Sánchez Llamazares, C. F. Sánchez-Valdés, Y. D. Zhang, C. Esling, X. Zhao, and L. Zuo, *Appl. Phys. Lett.* **100**, 174102 (2012).
- ²⁹K. A. Gschneidner, Jr., V. K. Pecharsky, A. O. Pecharsky, and C. B. Zimm, *Mater. Sci. Forum* **315–317**, 69 (1999).
- ³⁰M. E. Wood and W. H. Potter, *Cryogenics* **25**, 667 (1985).
- ³¹V. K. Pecharsky, J. O. Moorman, and K. A. Gschneidner, Jr., *Rev. Sci. Instrum.* **68**, 4196 (1997).
- ³²V. K. Pecharsky and K. A. Gschneidner, Jr., *J. Appl. Phys.* **86**, 565 (1999).
- ³³H. Oesterreicher and F. T. Parker, *J. Appl. Phys.* **55**, 4334 (1984).
- ³⁴V. S. R. de Sousa, E. J. R. Plaza, M. S. Reis, B. P. Alho, A. M. G. Carvalho, S. Gama, N. A. de Oliveira, and P. J. von Ranke, *J. Magn. Mater.* **321**, 3462 (2009).
- ³⁵Q. Y. Dong, J. Chen, J. Shen, J. R. Sun, and B. G. Shen, *Appl. Phys. Lett.* **99**, 132504 (2011).
- ³⁶B. Li, W. J. Hu, X. G. Liu, F. Yang, W. J. Ren, X. G. Zhao, and Z. D. Zhang, *Appl. Phys. Lett.* **92**, 242508 (2008).
- ³⁷L. Li, K. Nishimura, and H. Yamane, *Appl. Phys. Lett.* **94**, 102509 (2009).
- ³⁸P. Kumar, N. K. Singh, A. K. Nayak, A. Haldar, and K. G. Suresh, *J. Appl. Phys.* **107**, 09A932 (2010).
- ³⁹A. M. Gomes, I. S. Oliveira, A. P. Guimarães, A. L. Lima, and P. J. von Ranke, *J. Appl. Phys.* **93**, 6939 (2003).
- ⁴⁰W. J. Hu, J. Du, B. Li, Q. Zhang, and Z. D. Zhang, *Appl. Phys. Lett.* **92**, 192505 (2008).
- ⁴¹J. Chen, B. G. Shen, Q. Y. Dong, F. X. Hu, and J. R. Sun, *Appl. Phys. Lett.* **96**, 152501 (2010).
- ⁴²J. L. Wang, S. J. Campbell, J. M. Cadogan, A. J. Studer, and R. Zeng, *Appl. Phys. Lett.* **98**, 232509 (2011).